

FAILURE OF TUNGSTEN HEAVY ALLOYS SUBJECTED TO DYNAMIC TRANSVERSE LOADING

K. Tarcza^{1,2}, S. J. Bless*¹, and E. Taleff³

¹ Institute for Advanced Technology, University of Texas at Austin

² now at SFAE-AMO-MAS-SCI, Picatinny Arsenal

³Department of Mechanical Engineering, University of Texas at Austin

ABSTRACT

A new type of experiment has been developed to subject rods to dynamic transverse impact similar to that encountered in attack of modern armors. Two tungsten alloys with five different surface finishes were examined. It was found that there were two failure modes: one involved transverse fracture that initiates from surface flaws. The other was a consequence of gouge instability on the sliding surface. Polishing suppressed the first mode and enhanced the second.

1. INTRODUCTION

One of the challenges facing FCS is adequate lethality from a relatively light main gun. For long rod projectiles and simple armor targets (rolled homogeneous armor (RHA)), penetration is proportional to length. For fixed energy, penetration into a target increases as the length-to-diameter ratio (L/D) to the 2/3 power. Design of penetrators, thus, reduces to the problem of making the L/D ratio as high as possible.

However, for modern armors that employ moving plates, the situation is a great deal more complex. Penetrators are subjected to intense transverse loading which can lead to fracture. The optimized penetrator design becomes a compromise between large diameter to resist transverse fracture and long length for penetration.

A very serious obstacle to efficient design of penetrators is the lack of understanding of the dynamics of transverse fracture. There are no agreed-upon test procedures for determining fracture resistance, there are no techniques to predict transverse loads, there are no available fracture criteria for use in numerical simulations, and there are no standard strategies for engineering of penetrators to resist transverse fracture.

Against this backdrop, the development of a new category of gun—the electromagnetic railgun (EMG)—is taking place. The EMG is currently under consideration for the Block 2 FCS upgrade. EMGs make available much higher muzzle velocities than conventional powder

guns. This has led to a consideration of the effects of velocity on efficiency of long rod penetrators, with the results shown in Figure 1, which is based on the penetration formula for tungsten heavy alloy (WHA) rods found in Subramanian et al. [1]. The evident conclusion from the figure is that, for RHA penetration with a fixed L/D WHA rod, the most efficient impact velocity is about 2.2 km/s.

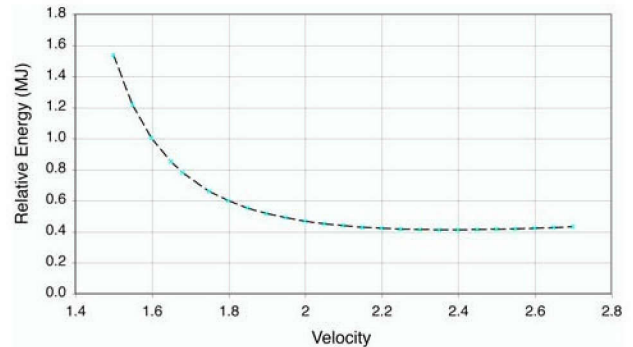


Figure 1. Relative energy required to penetrate a fixed distance of RHA with a constant-shape WHA rod.

The Institute for Advanced Technology (IAT) is the US Army R&D team concerned with developing penetrators for EMG. Thus have we come to focus on effects of transverse loads resulting from hypervelocity impact of WHA onto RHA elements.

2. MATERIALS

The microstructure of tungsten heavy alloys typically consists of relatively isolated W grains contained in a continuous matrix of a solid-solution alloy, such as Fe-Ni or Co-Ni. Modern penetrator alloys are 90–95 wt. % W, with Ni and either Fe or Co in a 7:3 weight-percent ratio. These alloys are most commonly processed by liquid-phase sintering, producing W grains with average diameters of 20–50 μm , as largely influenced by sintering time and temperature.

Two WHAs were employed in this investigation. One was a WNiFe alloy provided in the form of 32 mm

Report Documentation Page

Form Approved
OMB No. 0704-0188

Public reporting burden for the collection of information is estimated to average 1 hour per response, including the time for reviewing instructions, searching existing data sources, gathering and maintaining the data needed, and completing and reviewing the collection of information. Send comments regarding this burden estimate or any other aspect of this collection of information, including suggestions for reducing this burden, to Washington Headquarters Services, Directorate for Information Operations and Reports, 1215 Jefferson Davis Highway, Suite 1204, Arlington VA 22202-4302. Respondents should be aware that notwithstanding any other provision of law, no person shall be subject to a penalty for failing to comply with a collection of information if it does not display a currently valid OMB control number.

1. REPORT DATE 00 DEC 2004	2. REPORT TYPE N/A	3. DATES COVERED -			
4. TITLE AND SUBTITLE Failure Of Tungsten Heavy Alloys Subjected To Dynamic Transverse Loading		5a. CONTRACT NUMBER			
		5b. GRANT NUMBER			
		5c. PROGRAM ELEMENT NUMBER			
6. AUTHOR(S)		5d. PROJECT NUMBER			
		5e. TASK NUMBER			
		5f. WORK UNIT NUMBER			
7. PERFORMING ORGANIZATION NAME(S) AND ADDRESS(ES) Institute for Advanced Technology, University of Texas at Austin now at SFAE-AMO-MAS-SCI, Picatinny Arsenal; Department of Mechanical Engineering, University of Texas at Austin		8. PERFORMING ORGANIZATION REPORT NUMBER			
		10. SPONSOR/MONITOR'S ACRONYM(S)			
9. SPONSORING/MONITORING AGENCY NAME(S) AND ADDRESS(ES)		11. SPONSOR/MONITOR'S REPORT NUMBER(S)			
		12. DISTRIBUTION/AVAILABILITY STATEMENT Approved for public release, distribution unlimited			
13. SUPPLEMENTARY NOTES See also ADM001736, Proceedings for the Army Science Conference (24th) Held on 29 November - 2 December 2005 in Orlando, Florida. , The original document contains color images.					
14. ABSTRACT					
15. SUBJECT TERMS					
16. SECURITY CLASSIFICATION OF:			17. LIMITATION OF ABSTRACT UU	18. NUMBER OF PAGES 8	19a. NAME OF RESPONSIBLE PERSON
a. REPORT unclassified	b. ABSTRACT unclassified	c. THIS PAGE unclassified			

diameter bar stock. The other, a WNiCo alloy, was obtained in 12.7-mm (0.5-in) diameter bar stock. Nominal property data are summarized in Table 1.

Table 1: WHA Property Data

Alloy	93W-5.6Ni-1.4Fe	91.2W-6Ni-2.8Co
Manufacturer	OSRAM-Sylvania	Aerojet Ordnance
Designation	WN308F	Aero-224W
Sintered Density	17.76 g/cc	17.54 g/cc
Processing*	LPS, 20% Swaged	LPS, Proprietary
Elastic Modulus	362 GPa	365 GPa
Tensile Yield Strength (0.2%)*	1186 MPa	958 MPa
Ultimate Tensile Strength*	1255 MPa	1227 MPa
Elongation*	14%	24.5%

* manufacturer-provided data

Because both alloys were swaged and there is little mention in the literature of radial property variation as a result of swaging or its effect on performance, microstructural analysis was conducted on samples of virgin bar stock from each material to determine if there were radial differences in microstructure, and to measure grain sizes and aspect ratios. The techniques used for sample preparation are described in Tarcza [2004].

Results are shown in Fig. 2. Each material is remarkably homogenous. The WNiCo alloy has a notably finer W grain size than the WNiFe alloy.

3. SURFACE FINISH

A goal of the present study was to determine the effect of various surface-finishing techniques upon the failure behavior and fracture morphology of WHA rods. These included: electric-discharge machined (EDM) rods from large bar stock; EDM, then mechanically superpolished (SP) rods (prepared by hand using stainless steel buffing compound with cotton buffing wheel); EDM, then electropolished (EP) rods; EDM, then centerless ground (CG) between opposing grinding wheels resulting in round rods of uniform diameter throughout their length; and EDM, then CG, SP, and EP rod, for a total of five distinct surface finishes:

The measured properties of the specimens are summarized in Table 2. It was found that there was a fundamental difference in the nature of the different surface finishes, causing them to fall into two distinct categories: those with processing-induced surface damage and those without. Upon close SEM examination of the EDM, SP, and EP surfaces of both alloys, it became apparent that significant damage existed in the form of extensive microcracking of W grains. EP surfaces offer the best example of this, having effectively removed the EDM residue layer from the surface and revealing the true nature of the base material. In the EP surface micrograph in Fig. 3, fully 33% of complete surface grains in the image (20 out of 60) are either flawed or associated with flaws. The surface flaws were introduced by the EDM cutting. Only the CG and CG-SP-EP finishes totally removed the layer of cracked surface grains. Details of the effects of surface preparation can be found in Tarcza [2004].

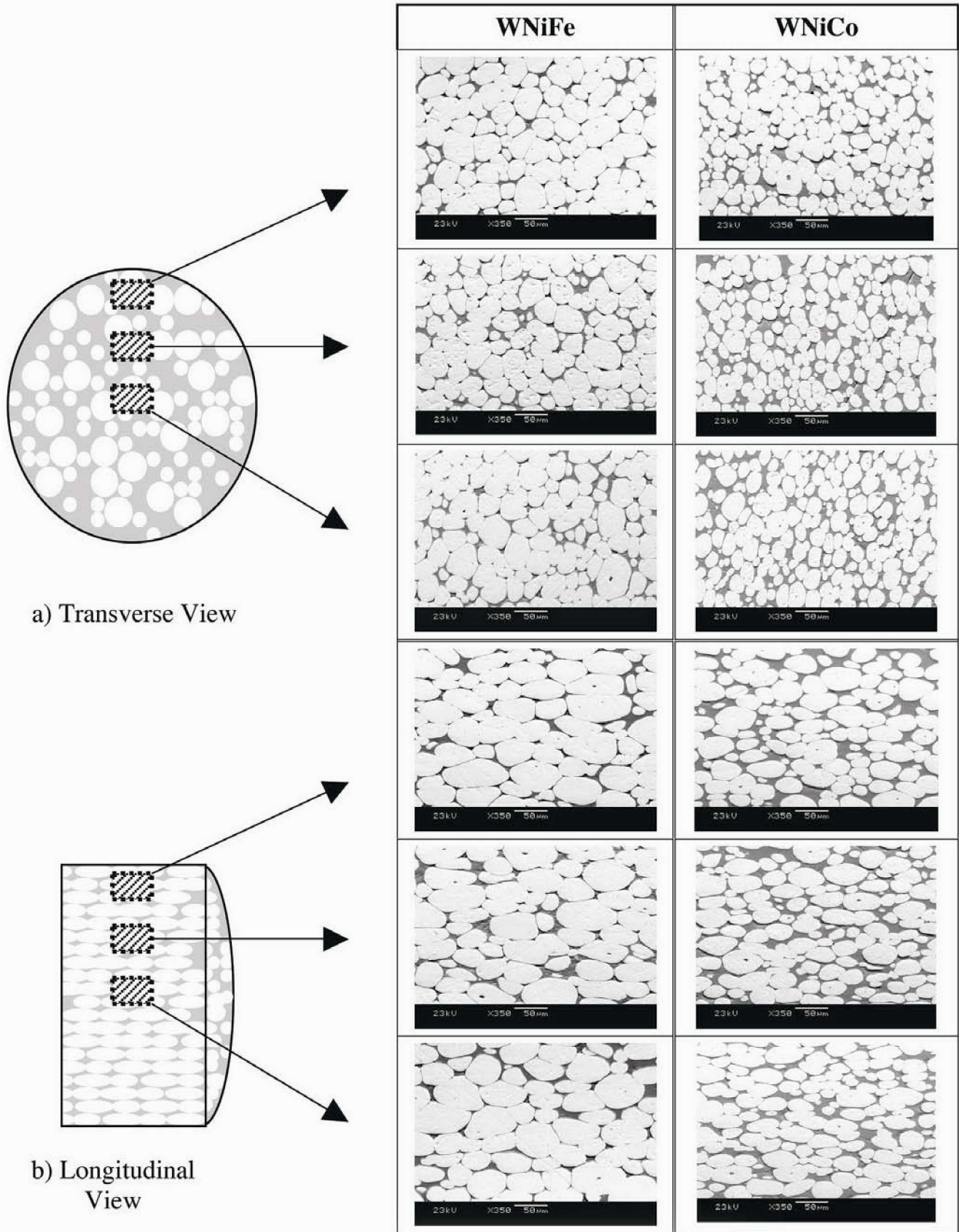


Figure 2. Microstructure of the as-received tungsten stock

Table 2. WHA Rod Parameter Variation Due to Surface Finish Enhancement

Alloy	Parameter	EDM	SP	EP	CG	CG-SP-EP
WNiFe	Average initial diameter (mm)	3.039	3.037	3.039	3.044	3.037
	Average diameter reduction from finishing (mm)	-	0.010	0.049	0.294	0.306
	Average resultant diameter (mm)	3.039	3.026	2.991	2.751	2.730
	Average initial mass (g)	13.912	13.905	13.922	13.900	13.886
	Average mass loss from finish (g)	-	0.094	0.442	2.485	2.626
	Average resultant mass (g)	13.912	13.811	13.48	11.415	11.26
	Number of rods prepared	62 ttl.	10	5	10	5
WNiCo	Average initial diameter (mm)	3.055	3.084	3.081	3.039	3.034
	Avg. dia. reduction from finishing (mm)	-	0.012	0.030	0.259	0.260
	Average resultant diameter (mm)	3.055	3.072	3.051	2.781	2.774
	Average initial mass (g)	13.912	14.161	14.138	13.735	13.690
	Average mass loss from finish (g)	-	0.107	0.274	2.238	2.244
	Average resultant mass (g)	13.912	14.055	13.864	11.497	11.446
	Number of rods prepared	36 ttl.	5	5	10	5

4. HIGH-SPEED TRANSVERSE IMPACT TESTS

Our principal interest was to observe damage caused by high-speed transverse impact, such as arises when a rod flying with an angle of attack hits a stationary target, or when an explosively launched flyer plate hits the side of a rod. The problem is that in these “direct ballistics” events, recovery of the projectile for inspection is virtually impossible. To get around this problem, high speed reverse impact tests were conducted using IAT’s two-stage light-gas gun. The impact geometry is shown in Figure 4.

WHA rods 108 mm long were used in reverse ballistic testing. The diameters are given in Table 2. They were held in a specially designed fixture that also promoted recovery of specimens after impact.

The launch packages consisted of RHA cylinders that were press-fit into Lexan™ sleeves. Initially, each launch package had an approximate mass of 420 g with outer dimensions of 38.1 mm in diameter and 69.85 mm in length (including the Lexan™). After preliminary tests, the design was modified to include a two-piece detachable sleeve to ensure that initial contact between a

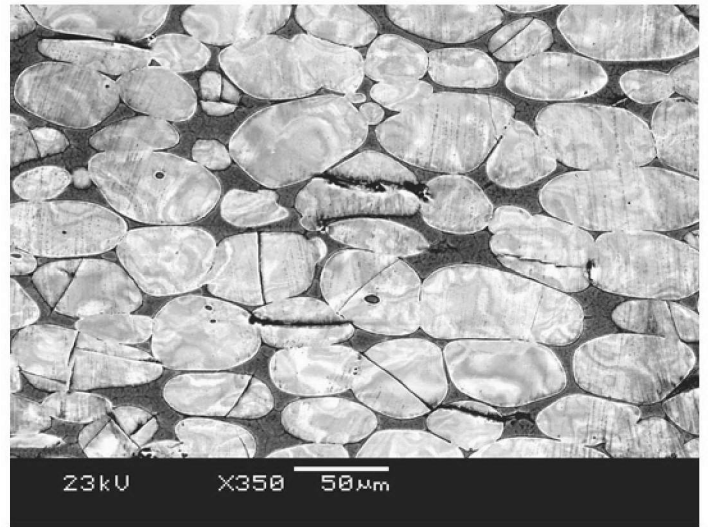


Figure 3. SEM surface micrograph of EP WNiFe

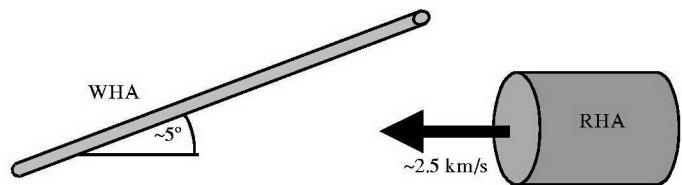


Figure 4. Reverse impact setup.

rod and the sleeve was avoided. Slightly increasing the sleeve thickness and reducing the core diameter as a result dropped the mass to 360 g while maintaining the exterior dimensions. The impact simulates a yawed rod impact onto a thick RHA target. The first part of the impact, which produces a crater, is avoided. However, the side of the rod comes in contact with the steel cylinder and cuts a slot in the cylinder. This is identical to what happens in a forward-ballistics yawed rod impact when the rod comes in contact with the sidewall of the crater. As the rod cuts a channel into the steel, the reaction forces from the steel deflect the rod. The mechanical response of the rod is the same as if it had hit a stationary target while flying with an angle of attack. It is also identical to the response of a rod struck by a transversely-moving flyer plate. Both scenarios are of great practical interest to the Army.

5. RESULTS OF EXPERIMENTS

Twenty-three experiments were conducted. The velocities were in the hypervelocity regime that is of most interest to EMG systems that are candidates for FCS upgrades.

The general response of rods is to be thrown into an arc trajectory. The initial part of the rod that misses the steel block is undeflected. However, the lateral force increases as the rod is more embedded into the plate – giving the back of the rod the highest transverse velocity. The x-rays are taken soon after exit from the plate, so the gentle curvature of the rod shown in the x-rays does not wholly reflect the fact that the back of the rod has experienced a more violent event than the front. This idealized behavior of the rod is most easily shown in a numerical simulations, displayed here in Fig. 5 (from Fuentes, 2003), where it is compared to an experimental result from Shot 717, conducted at 2.3 km/s with EDM WNiFe material.

The actual tungsten rods emerged from the target with multiple fractures, as shown in Fig. 6. These fractures are initiated under tensile loading, typically on the side of the rod opposite that interacting with the target. Fractures deflect gradually toward the rod tail, the direction of sliding load motion, developing a characteristic lazy-S shape. The one exception to this is shown in Fig. 6 fracture #4, caused by initial rod-launch package contact in the vicinity of fracture #3, which forced the nose of the rod to whip clockwise. This generated a backwards-fracture running from bottom to top, opposite from the fractures caused by the rod bending in response to contact with the launch package, such as in fractures 1–3 in Fig. 6. The rod segments have a fairly uniform size, with an average mass of 1.0 g as determined from recovered fragments.

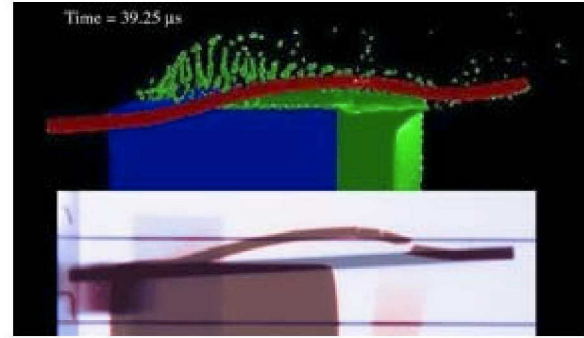


Figure 5. Upper: CTH simulation of rod showing leading part that missed the block, next part that has been deflected, and trailing part that is still within slot. Lower: Shot 717: x-ray superposition of initial position of rod and dynamic deflection of rod.

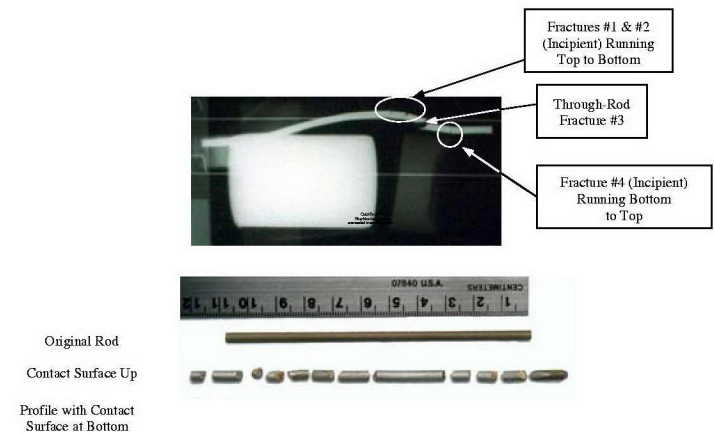


Figure 6: Recovered fragments from shot 717.

The results of the above experiments can be explained in terms of fracture of a rod that was deflected by the cavity stress in the target, deformed in flight, and fractured due to the bends that resulted from transverse velocity gradients.

An entirely different failure mode was observed, for example, in Shot 757, shown in Fig. 7. In this experiment, the slot-cutting process has become unstable. There resulted a violent disruption that produced locally very high velocity gradients and very fine fragmentation of the rod. Figure 8 shows the fragments recovered from shot 757. The fractures involve axial splitting of the rod, as opposed to the transverse rupture that occurs normally.

Through examination of the recovered fragments and comparison with flash x-ray photographs, it became evident that the debris plumes were the result of hypervelocity gouging. Gouging has been previously

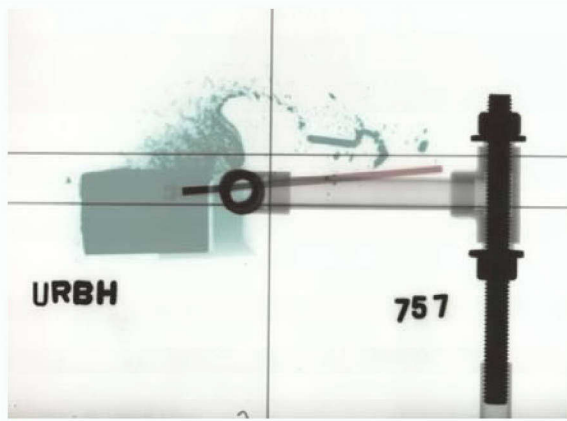


Figure 7. X-ray of deflected rod in Shot 757.

observed to occur in thin-plate penetration by tungsten rods [Satapathy et al., 2003]. Rod gouges have a shiny, distorted appearance, indicating the extreme loading conditions under which they are created, and the characteristic teardrop shape. They initiated uprange and always resulted in rod failure.

6. EFFECT OF SURFACE FINISH

There was a strong correlation between the surface finish and the failure mode. This is shown in Figure 9. The specimens with more highly polished surfaces were more prone to gouging failures and less prone to transverse fracture.

7. METALLOGRAPHIC ANALYSIS

Extensive metallographic analysis was conducted on the recovered fragments (Tarcza, 2004). Only the broadest features of those observations are discussed in this paper.

Surface damage accumulation has been observed to be most significant adjacent to fractures which lead to rod failure. In the case of reverse ballistic specimens, this is particularly true for damage accumulation on the up-range side of a fracture toward the tail end of rod pieces. In considering the surface condition extremes for the two alloys, EDM and CG-SP-EP, it was clear that EDM specimens were dominated by surface-initiated W grain cleavages, though the WNiCo alloy did exhibit a limited number of internal cleavage sites. Although depths of penetration into the body of the rod varied, observations



Figure 8. Fragments recovered from shot 757.

of the distribution of fractures initiated on tensile surfaces after reverse ballistic tensile surfaces show the largest cracks to be uniformly spaced approximately 200 μm apart. In contrast, CG-SP-EP surface improvement greatly reduces the damage visible at a 90x magnification for both alloys, and the largest fractures are linked W grain cleavages nucleated in the interior of the rod segments, as shown in Fig. 10. In the case of the WNiCo specimens, the proximity of internal fractures to the tail end of the segment and the absence of any other incipient fractures makes a strong case for rod failure from internally nucleated damage; this is less clear for the WNiFe CG-SP-EP specimen.

Recovered specimens with gouges were examined. Transient loading induced by high velocity sliding contact acts first at a discrete location, triggering an expanding region of significant plastic surface deformation. Contact conditions become more severe as the gouge region expands, leading to surface melting and material removal, as well as gross W grain deformation. This causes a scaly, smeared appearance as W grains are elongated, flattened, and overlapped, as shown in Fig. 11(a). Contact surfaces on the rod and target are expected to gouge simultaneously, and material from the growing crater(s) is drawn downrange as the transient load begins to diminish. Gouges terminate with a lip of this material pushed up at the tail end of the gouge as shown in Fig. 11(b), followed by the region of gradually diminishing surface melting and solidification seen in Fig. 11(c). As steady-state contact conditions resume, the surface reverts to the more usual, scoured appearance of Fig. 11(d).

8. CONCLUSION

Slot cutting, as occurs in hypervelocity impact with AOA or against moving-plate targets, results in projectile deflection and bending. For 3-mm diameter tungsten rods impacting at hypervelocity, there are two macro response modes—one is isolated transverse fractures, the other gouging leading to violent fragmentation. Transverse fracture occurs primarily by grain cleavage, which initiates at surface flaws if they are present. Gouging incites axial splitting. Fracture is strongly influenced by surface finish. Highly polished surfaces are more resistant to transverse fracture, but may fail by gouging, which is more catastrophic in terms of ultimate penetrator performance.

	WNiFe	WNiCo
EDM		
SP		
EP		
CG		
CG- SP- EP		

Figure 9. Deflected rod shapes and recovered fragments.

ACKNOWLEDGMENT

The research reported in this document/presentation was performed in connection with Contract number DAAD17-01-D-0001 with the US Army Research Laboratory. The views and conclusions contained in this document/presentation are those of the authors and should not be interpreted as presenting the official policies or position, either expressed or implied, of the US Army Research Laboratory or the US Government unless so designated by other authorized documents. Citation of manufacturer's or trade names does not constitute an official endorsement or approval of the use thereof. The US Government is authorized to reproduce and distribute reprints for Government purposes notwithstanding any copyright notation hereon.

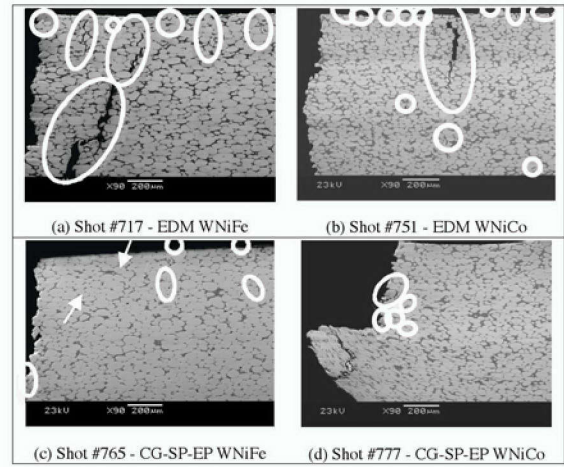


Figure 10. Normal cross sections of specimens with fracture initiation sites identified (tensile side on top).

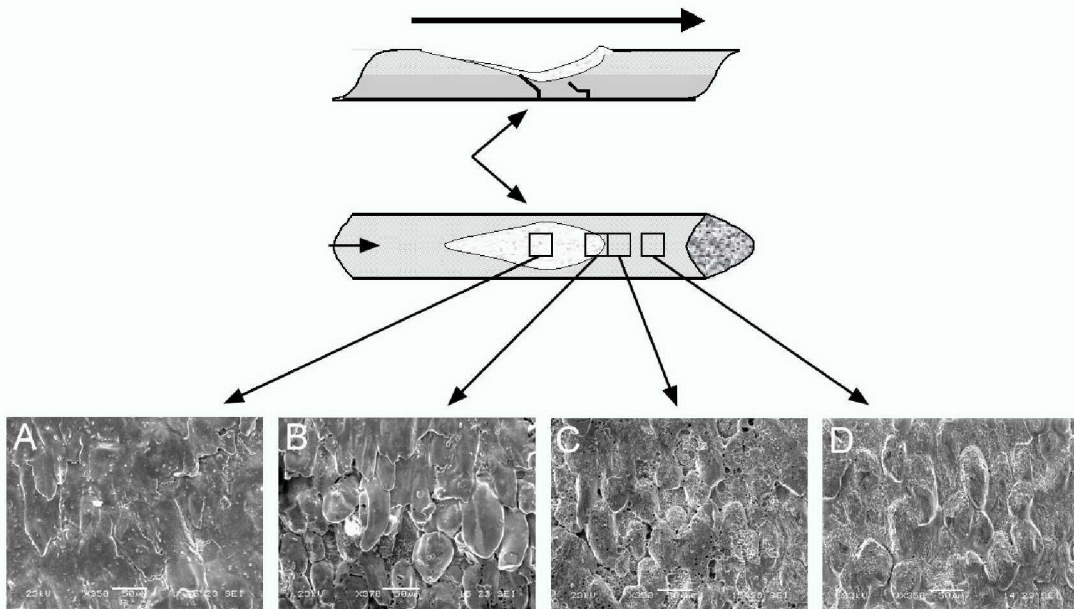


Figure 11. Examination of shot 757 gouge crater and nearby surface details. A) Gouge surface interior; B) Downstream gouge lip; C) Near beyond gouge; D) Far beyond gouge.

10. REFERENCES

- R. Subramanian, S. J. Bless, "Reference Correlations for Tungsten Long Rods Striking Semi-Infinite Steel Targets," 19th Int'l Symp. Ballistics, Interlaken, Switzerland, 7-11 May 2001
- D. Fuentes, unpublished, 2003
- S. Satapathy, C. Persad, R. Monfredo, and S. Bless, "On the Nature of Surface Modification Produced by Non-Planar Hypervelocity Sliding in Tungsten Alloy." Int. J. Impact Engng, Vol. 28, 621-630, 2003
- K. Tarcza, "The Dynamic Failure Behavior of Tungsten Heavy Alloys Subjected to Transverse Loads," Dissertation, Univ. of Texas at Austin, August 2004.